lubricants

MDPI

Article

Contribution of Zn–Co Alloys Coatings Study: Electrodeposition Methodology, Micromechanical Properties, and Tribological Behavior

Faten Nasri [1], Dorra Trabelsi [1], Mohamed Kharrat [1,*], Maher Dammak [1], Antonio Pereira [2,*], César Cardoso [3] and Florence Vacandio [4]

[1] Laboratory of Electromechanical Systems (LASEM), National Engineering School of Sfax, University of Sfax, 3038 Sfax, Tunisia; nasrifaten85@gmail.com (F.N.); dorra.trabelsi.01@gmail.com (D.T.); maher.dammak@ipeis.usf.tn (M.D.)
[2] Centre for Mechanical Technology and Automation (TEMA), Department of Mechanical Engineering, University of Aveiro, 3810-193 Aveiro, Portugal
[3] Rodi Industries, S.A., 3801-551 Aveiro, Portugal; ccardoso@rodi.pt
[4] Laboratory “Divided Materials, Interface, Reactivity, Electrochemistry” (MADIREL), Aix-Marseille University, 13331 Marseille, France; florence.vacandio@univ-amu.fr
* Correspondence: mohamed.kharrat@ipeis.usf.tn (M.K.); abastos@ua.pt (A.P.)

Abstract: An overview of the literature reveals that electrodeposition baths significantly influence deposited coatings’ morphology and properties. The present study investigates a sulphate-based bath in terms of the additive, pH, and temperature for the electrodeposition of Zn–Co alloys onto mild steel, achieving a nanocrystalline structure. The obtained results of the cyclic voltametric and SEM analyses revealed that sodium allowed the enhancement of cobalt electrocrystallisation (22.6 wt%) to homogenize further layers’ structure. However, the adjustment of pH allowed for the obtention of deposits with a refined structure containing only 5 wt% cobalt. Although an increase in room temperature resulted in deposit coatings with the same cobalt content, it notably produced a smoother structure. Subsequently, Zn–Co coatings were compared to pure zinc layers in terms of micromechanical and tribological behaviour. The morphology shifted from hexagonal platelets to nodular structures with the incorporation of cobalt, leading to an increase in microhardness. The morphology transformation, coupled with micromechanical reinforcement, contributed to the mitigation of friction and the improvement of the wear resistance of zinc layers through cobalt alloying. In fact, this improvement enhances the performance of zinc-coated applications in automotive and aerospace industries, particularly for standard assembly components that require adequate resistance to wear and abrasion during handling and tightening.

Keywords: Zn–Co coatings; bath parameters; temperature; cyclic voltametric study; tribology; microhardness

check for updates

Received: 7 March 2025
Revised: 26 March 2025
Accepted: 1 April 2025
Published: 7 April 2025

Citation: Nasri, F.; Trabelsi, D.; Kharrat, M.; Dammak, M.; Pereira, A.; Cardoso, C.; Vacandio, F. Contribution of Zn–Co Alloys Coatings Study: Electrodeposition Methodology, Micromechanical Properties, and Tribological Behavior. *Lubricants* **2025**, *13*, 167. https://doi.org/10.3390/lubricants13040167

1. Introduction

Substantial attention has been drawn to zinc alloy coatings (Zn–Ni, Zn–Co, Zn–Fe. . .) as a feasible solution to ameliorate the features of zinc layers in terms of corrosion behaviour and wear resistance [1–4]. Research on these alloys is regularly evolving thanks to their practical applications, especially in the automotive industry [5,6]. Several methods are currently suggested to improve the characteristics of Zn–Co layers, namely the incorporation of solid particles and the use of ion liquids as electrodeposition baths [7–10], because coating behaviour has always been determined by the layers’ features. Hence, researchers constant endeavour has been to enhance the qualities of these coatings, highlighting key elements such as morphology, microstructure, and grain-size characteristics [11–14]. The relentless pursuit of optimizing the deposition conditions on Zn–Co coating aspects have been proven to improve the layer properties.

Hence, the deposition conditions of these coatings and their properties have been explored by many studies, demonstrating the substantial effect of several parameters such as bath composition, additives, pH, temperature, agitation, and current density on their quality [15–17]. Indeed, additives in the electrodeposition process have been of interest in many research works. In fact, a variety of additives has been used for distinct research purposes. In some cases, a single additive was added, while in other cases, a series of additives were incorporated into the bath deposition. The use of additives was accompanied by the appropriate choice of pH, agitation, temperature, etc. In this context, while Ortiz et al. [14] have used a complicated bath that incorporates many additives such as KCl, H3BO3, benzylidene acetone, PEG8000, etc., Garcia et al. have deployed only $Na_3C_5H_6O_7$ as an additive [18]. Furthermore, zinc and cobalt concentrations have been confirmed to have a significant effect on the Zn–Co coating morphology and microstructure, and therefore on its performance [19]. The extensive use of different parameters such as the additive pH can be justified by the fact that varying electrodeposition baths result in different Zn–Co coating morphologies, even when a similar cobalt content is present. For example, studies conducted by Lodhi et al. [20] using acidic chloride electrolytes have found an angular grain morphology for 1 wt% cobalt. However, other researchers employing a sulphate-based bath found that Zn–1.5 wt% Co coatings exhibited a nodular and fine structure [21]. Furthermore, Lodhi et al. reported that alloy films with 15 wt% cobalt displayed two distinct regions with some cauliflower-like formations [20]. In contrast, using a different deposition bath, Kahloul et al. developed layers with a similar cobalt content but a homogeneous surface and nodular structure [22]. Therefore, a great deal of research in the literature has corroborated the key role of bath composition and parameters in the development of films, mainly with a fine morphology and single-phase structure, which boosts the micromechanical properties and corrosion resistance of these coatings [5,23].

Unlike the study of coatings electrodeposition process, to the best of our knowledge, research examining the micromechanical characteristics and tribological behaviour of Zn–Co alloys coatings are limited. In fact, Panagopoulos et al. [24] studied the tribological behaviour of Zn–Co electrodeposited coatings on copper substrates, indicating that the surface delamination mechanism was the principal wear mechanism for Zn–4 wt% Co coatings. In addition, other studies [12,25] investigated the microhardness and adhesion properties of Zn–Co electrodeposits on mild steel with different thickness. Moreover, Panagopoulos et al. [25] proved that the more a layer thickness increased, the more the bond of the Zn–Co coatings to the substrate weakened, namely due to the increase in residual stress in these coatings. Further studies [12,21] have focused on mechanical properties in terms of tensile strength, yield strength, and the modulus of elasticity.

In the present study, we selected a basic sulphate bath, as referenced in the literature, to develop Zn–Co coatings with a high cobalt content [24,25]. In the previous works [24,25], two types of Zn–4 wt% Co films were produced using this bath. Regarding the first type, it was deposited on copper and analyzed for microhardness and tribological behaviour using pin-on-disc wear apparatus [24]. However, the second type was developed on mild steel as a substrate to investigate only its micromechanical properties, specifically in terms of microhardness [25]. The morphology of the latter exhibited a few microcracks with a non-typical nodular structure. The basic sulphate bath used for Zn–Co layer deposition included sodium sulphate (Na_2SO_4) as an additive, maintained a pH of 1.5, and operated at 20 °C. However, neither study explored the influence of electrodeposition parameters such as the additive, pH, or current density. Additionally, these Zn–Co coatings were not compared to pure zinc developed under similar conditions.

In the present work, Zn–Co coatings were electrodeposited from a sulphate-based bath mentioned in the literature, using mild steel as the substrate. The impact of bath conditions was exposed to obtain nodular and fine structure with a single-intermetallic phase. The obtained coating alloys were subsequently compared to pure zinc coating in terms of morphology, microstructure, micromechanical, and tribological features. Tribological tests were conducted using a reciprocating tribometer.

2. Materials and Methods

To produce the coatings under study, the electrodeposition process was employed using the chemical solutions of the used baths, deposition parameters, anode, and cathode listed in Tables 1 and 2, and vitreous carbon and mild steel as substrates. According to Table 1, each parameter, including the additive (sodium sulphate), was analyzed to determine its role in the electrolytic bath during the deposition process. This study was conducted under consistent conditions, with applied potential (−1.2 V), room temperature (17 °C), platinum as the anode, and a saturated calomel electrode (SCE) as the reference electrode (SCE). However, different cathodes were employed. Firstly, vitreous carbon was employed to study the effect of sodium, but in the subsequent steps the electrodeposition was performed directly onto mild steel, which was the chosen substrate for studying the coatings properties in the present work. The influence of room temperature on coatings deposition, with an adjusted pH and sodium addition, was evaluated by increasing the room temperature from 17 to 24 °C. As shown in Table 2, the temperature effect was studied under similar conditions consistent with the additive and pH settings. These conditions were also applied to the development of pure zinc and Zn–Co alloy films. Furthermore, Table 2 highlights the current density and plating time required to produce the investigated coatings with a thickness of 50 µm. These are also highlighted in Table 2. A summary of the electrodeposition methodology for the different investigated coatings is presented in Figure 1. While the specimens used for investigating the coating morphology had dimensions of 10 × 10 × 5 mm^3, those employed for mechanical and tribological characterizations measured 30 × 15 × 20 mm^3. Before each deposition process, the mild steel substrate was mechanically polished using SiC paper with grits ranging from 180 to 1000 and then activated in HCL. It was then entirely rinsed with ionized water and ethanol.

Table 1. Sulphate bath conditions used for the electroplating of Zn–Co alloy coatings under 17 °C.

Bath Composition (g/L)			
$ZnSO_4 \cdot 7H_2O$ (150)/$CoSO_4 \cdot 6H_2O$ (350)			
Operating Conditions			
Solutions	**(A)**	**(B)**	**(C)**
Room Temperature (°C)	17		
$Na_2SO_4 \cdot 6H_2O$ (g/L)	-	75	75
Applied Potential (E, V)	−1.2	−1.2	−1.2
pH	2.5	2.5	1.7
Electrolyte Volume (mL)	250	250	250
Anode	Platinum	Platinum	Platinum
Cathode	Vitreous Carbon	Vitreous Carbon	Mild Steel
ReferenceEelectrode	Saturated Calomel (SCE)	Saturated Calomel (SCE)	Saturated Calomel (SCE)

Table 2. Sulphate bath conditions used for the electroplating of pure zinc and Zn–Co alloy coatings under 24 °C.

	Bath Composition (g/L)	
	$ZnSO_4 \cdot 7H_2O$ (150)/$CoSO_4 \cdot 6H_2O$ (350)	**$ZnSO_4 \cdot 7H_2O$ (150)**
	Operating Conditions	**Operating Conditions**
Solutions	**(D)**	**(E)**
Room Temperature (°C)	24 °C	
$Na_2SO_4 \cdot 6H_2O$ (g/L)	75	75
Applied Potential (E, V)	−1.2	−1.2
pH	1.7	1.7
Electrolyte Volume (mL)	250	250
Anode	Platinum	Platinum
Cathode	Mild Steel	Mild steel
Reference Electrode	Saturated Calomel (SCE)	Saturated Calomel (SCE)
Current Density (A/dm^2)	2	3.7
Plating Time (min)	90	64
Thickness (µm)	50.0 ± 0.5	51.0 ± 1.0

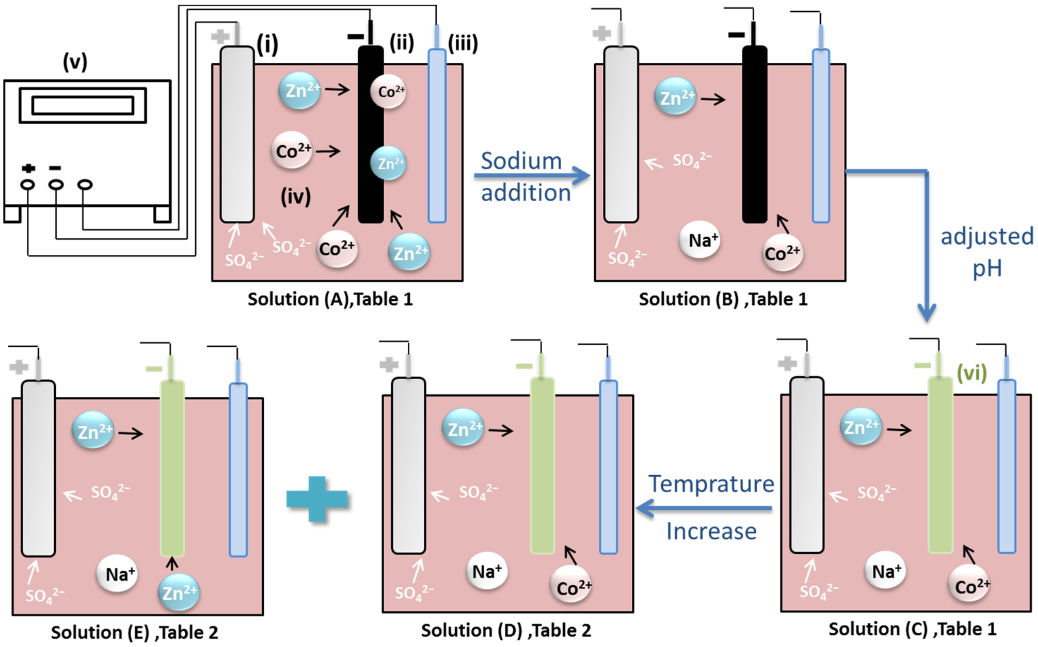

Figure 1. Schematic of the electrodeposition methodology for the different investigated coatings: (i) anode, (ii) cathode 1 (vitreous carbon), (iii) reference electrode (SCE), (iv) electrolyte, (v) power source, (vi) cathode 2 (mild steel).

A cyclic voltametric study was used to identify the current density J (A/cm^2) of the solution according to the applied potential E (V). The potential varied from cathodic to anodic potentials at a given scan speed (20 mV/s). Cyclovoltamograms obtained by this study presented two parts: a cathodic peak corresponding to the reduction in investigated chemical elements (Zn, Co. . .) and an anodic peak corresponding to their oxidation. The obtained curves made it possible to determine the decrease potentials of each element present in the bath.

We used a scanning electron microscope connected with an EDS facility to explore the surface morphology of elaborated coatings. In fact, the EDS analysis allowed for the estimation of the deposition rate of chemical elements (Zn, Co, etc.). This rate was confirmed by analyzing different samples of coatings deposited under similar conditions. In addition, we employed an X-ray diffractometer (XRD) Brucker–SIEMENS D5000 with Cu-ka radiation (k = 0.15440 nm) and a graphite monochromator to analyze the crystallographic structure: (Siemens/Bruker SAS, Karlsruhe, Germany). The obtained diffraction patterns were compared with the joint committee on powder diffraction standards (JCPDSs). Pattern analysis was performed using Diffract At Software (Diffracplus EVA). The average size of the crystallites in the developed coatings was then calculated using the Debye–Scherrer equation, which is as follows:

$$D = \frac{0.9\lambda}{\beta \cos\theta}$$

where λ is the wavelength of the X-ray radiation, θ is the Bragg angle of the peak, and β is the angular width of the peak at full width at half maximum (FWHM).

The measurement of the hardness was realized by the Vickers microhardness testing machine, employing the diagonals method and an applied load P of 1 daN. The average value considered was obtained from at least five tests conducted in distinct areas of each sample. To develop the tests, we made use of a diamond indenter in the shape of a square pyramid, with an angle between the edges denoted as $\alpha' = 136°$. For each test, the calculation of the hardness Hv was carried out from the measured value of the diagonal D footprint using the following expression [26]:

$$H_v = 1.854\frac{P}{D^2}$$

The friction and wear characteristics of the pure zinc and Zn–Co alloy coatings were measured by applying an alternating tribometer. The coated substrate came into contact with a high chromium steel ball (100Cr6, 15 mm in diameter) under a steady normal load of 6 N. The coated substrate underwent 5000 cycles of linear reciprocating motion at 1 Hz, with a displacement amplitude of ±7.5 mm. The tribological tests conducted were primarily aimed at comparing the friction and wear characteristics between the microstructured pure zinc coating and the nanostructured Zn–Co coating. A displacement amplitude of 15 mm (track length) was selected, which is representative of some automotive parts used in sliding contacts, namely a closing ratchet and master cylinder piston. To limit excessive contact heating, which can accelerate the oxidation of contact surface screens and third bodies (detached particles), a low frequency of 1 Hz was employed. A total of 5000 sliding cycles was chosen to ensure that a steady-state regime with a stable friction coefficient was reached. Finally, the normal load used was the lowest value adjustable on our device, chosen to minimize damage to the coating. Subsequently to each friction test, the stabilized value of the friction coefficient was determined and a transversal profile of the wear scar was established using an SJ-210 tactile profilometer (Mitutoyo, Aurora, IL, USA). The cross-section S (mm^2) of the groove was determined and the volume loss V (mm^3) was calculated using the following equation:

$$V = S \times d$$

where d is the length of the sliding track which is equal to 15 mm.

At least three friction tests were carried out on each coating.

3. Results and Discussion

3.1. Study of Sulphate Bath Parameters

3.1.1. Effect of Sodium as an Additive

The cyclovoltamograms of zinc (Zn) and cobalt (Co) in the absence (Table 1, Solution A) and presence of sulphate sodium (Table 1, Solution B) are displayed in Figure 2. At a sweep rate of 20 mV/s and pH of approximately 2.5, the cyclovoltamograms revealed the reduction/deposition (cathodic peak) and oxidation (anodic peak) of zinc (Figure 2a) and cobalt (Figure 2b). For the pure zinc, the cathodic peak reached −1.2 V, corresponding to −0.005 A/cm^2 as current density, both in the absence and presence of the additive. Concerning cobalt deposition, the cathodic peaks for both without and with sodium seemed to be similar, occurring at −1.2 V with a current density of approximately −0.023 A/cm^2. However, the anodic peak was more pronounced in the presence of sodium, exhibiting a current density of 0.019 A/cm^2 compared to 0.01 A/cm^2 without sodium. Indeed, the curves show that the addition of sodium has no remarkable outcome on pure zinc deposition (Figure 2a) regarding similar oxidation peaks. However, cobalt was greatly reduced in the presence of sodium, leading to a substantial increase in the oxidation peak (Figure 2b), indicating a higher cobalt content deposited due to the presence of sodium. The impact of sodium sulphate (Table 1, Solution B) on the Zn–Co alloys is illustrated in Figure 3. The addition of sodium sulphate appeared to have no effect on the cathodic peaks (−0.007 A/cm^2). In addition, three anodic peaks corresponding to the oxidation of chemical elements are depicted. The first peak is often caused by attributed to the dissolution of zinc from the Zn-rich phases that develop. The other two peaks are most likely associated with dissolution occurring after the preferential dissolution of zinc. The second outgoing peak at −0.6 V, corresponding to the deposit with added sodium, is more pronounced than that without sodium, as evidenced by the calculated charge density which increased from −0.0043 to 0.0065 C/cm^2. This peak is promoted, followed by a reduction in the intensity of the first peak corresponding to zinc dissolution. This may be explained by the preferential deposition of cobalt during the electrodeposition process in the presence of sodium sulphate. These findings suggest that, when comparing the two deposits, the reduction of both zinc and cobalt was significantly influenced by the presence of sodium.

Figure 4 depicts microscopic analyses of Zn–Co alloy coatings without and with the addition of sodium. Without sodium, the deposit exhibits a uniform surface covered with small clusters, indicating the presence of both zinc and cobalt, with zinc being predominant (Figure 4a) as confirmed by EDS analysis. At higher magnification, two different areas can be observed (Figure 4a′ and Figure 4a″). The first area (Figure 4a′) corresponding to the uniform surface consists of rounded particles trapped in hexagonal pellets, forming zinc plates. This suggests the start of the transformation from the hexagonal structural characteristic of pure zinc to a nodular morphology associated with Zn–Co alloys. In the second area (Figure 4a″), this transformation appears more pronounced, as the clusters exhibit a well-developed nodular morphology. In fact, the clusters present nodular morphology. These clusters fit together even more with the addition of sodium (Figure 4b). At low magnification, the surface seems to be less uniform. Two different phases are observed, and while the first part of the surface appears smooth the second one exhibits clusters. However, at high magnification, Zn–Co layers are more homogeneous with a nodular structure for both distinct phases (Figure 4b′ and Figure 4b″). The cobalt content augments from 16 to 22.6 wt% with sodium addition. In fact, the Zn–Co layers' morphology changes from rounded particles trapped in zinc plates to a perfectly nodular and more homogeneous structure, due to the accelerated Co reduction during electrodeposition. These observations support the findings of the cyclic voltametric study.

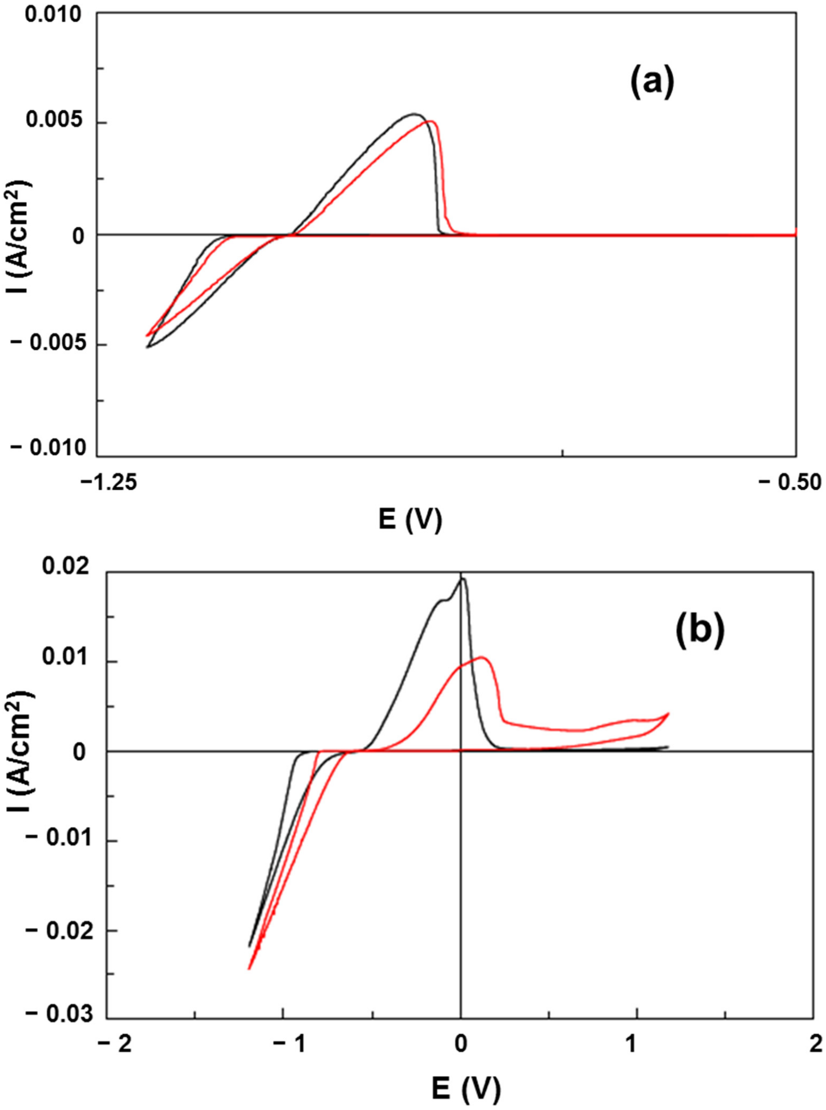

Figure 2. Cyclic voltametric of zinc (**a**) and cobalt (**b**) without (red) and with (black) additive.

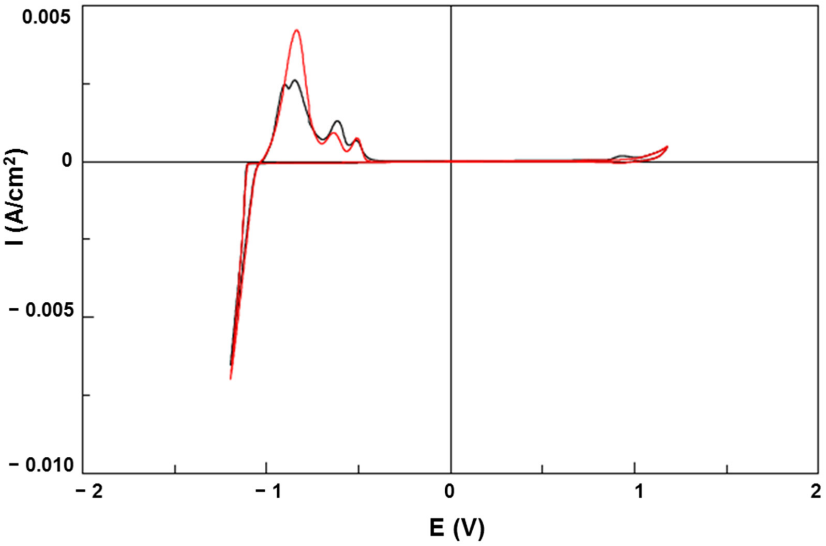

Figure 3. Cyclic voltametric of Zn–Co alloy layers without (red) and with (black) additive.

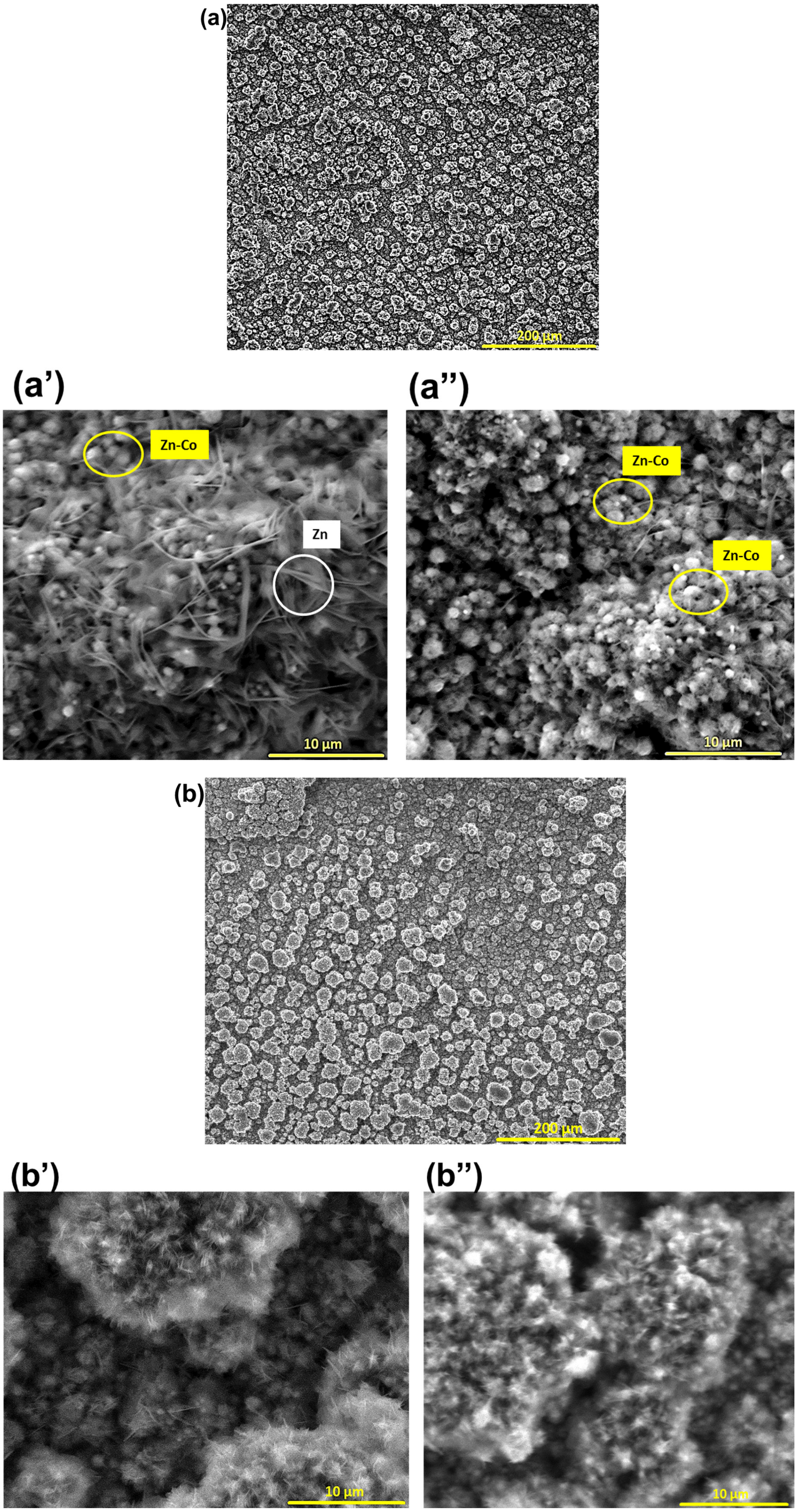

Figure 4. SEM micrographs of Zn–Co alloy layers for distinct areas without (**a**,**a′**,**a″**) and with (**b**,**b′**,**b″**) additive at different magnifications.

3.1.2. Effect of Adjusted pH

The pH effect (Table 1, Solution C) presented in Figure 5 shows that adjusting the pH to 1.7, compared to Figure 3, delays zinc and cobalt reduction, resulting in only two oxidation peaks. Regarding the first oxidation peak, it most likely corresponds to the zinc dissolution from the Zn-rich phases formed. As for the second one, it probably relates to the dissolution of Co left after the preferential dissolution of zinc. The latter peak is negligible compared with that of pure zinc.

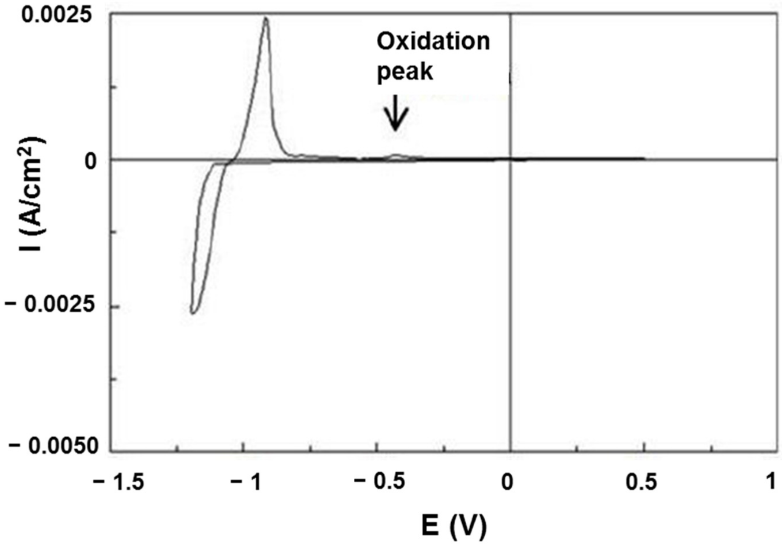

Figure 5. Cyclovoltamogram of Zn–Co alloy layers after pH adjustment.

As can be seen from Figure 6a, the SEM observation of the developed deposit after pH adjustment proves there to be a more homogeneous surface due to the increased consolidation of clusters. At high magnification (Figure 6b), microscopic observation discloses nodular morphology with a smoother surface compared to coatings deposited with the initial pH. The Co content dropped remarkably from 22.6% to 5 wt%, thus confirming the trivial peak revealed by cyclovoltamograms. Consequently, the pH allows the homogenization and refinement of the Zn–Co deposit, permitting only the reduction in two phases that normally correspond to pure zinc and the intermetallic phase.

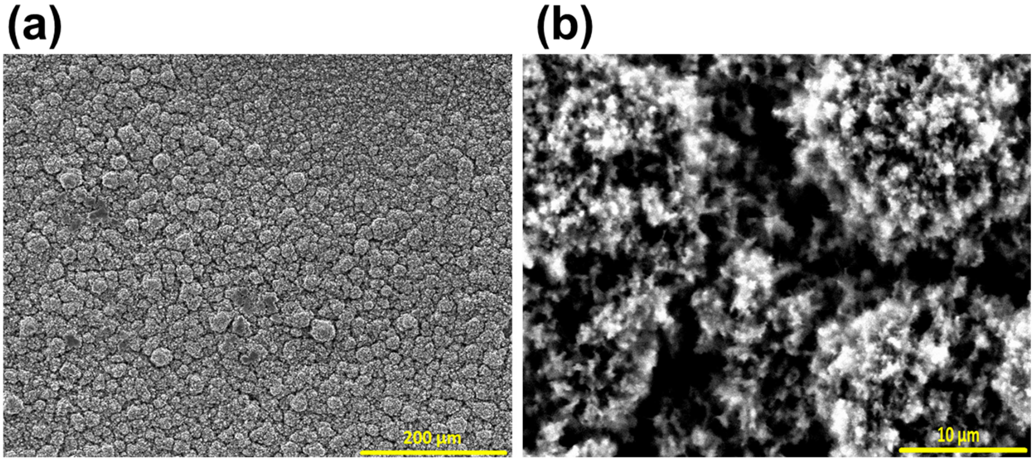

Figure 6. SEM micrographs of Zn–Co alloy layers after pH adjustment at different magnifications; (**a**): 250× (**b**): 5000×.

3.1.3. Effect of Temperature

The goal was to explore the effect of room temperature on the Zn–Co alloy deposition. In fact, using the following conditions of an adjusted pH, sodium addition, mild steel as substrate, and increasing the room temperature from 17 to 24 °C (Table 2, Solution D), leads to the SEM micrographs shown in Figure 7. By comparing this figure with Figure 6, (17 °C) it is clear that the room temperature has a considerable effect on the alloys' deposition. Indeed, the surface seems to be remarkably more uniform as the cluster size decreases, allowing for the deposit of coatings with a nodular and noticeably smoother structure. Nonetheless, the Co percentage does not alter, and the coatings still contain 5 wt% Co. Thus, increasing the ambient temperature allows for the refinement of the layer structure without changing the Co percentage.

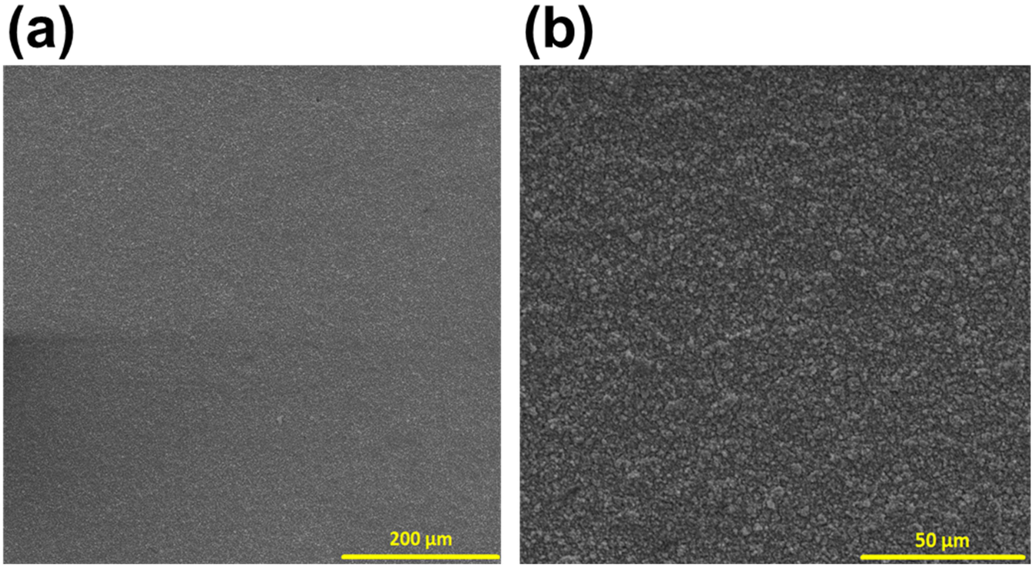

Figure 7. SEM micrographs of Zn–Co alloy layers at 24 °C at different magnifications; (**a**): 250× (**b**): 1000×.

Aiming to compare the last developed layers (Zn–Co alloy deposited at 24 °C) to pure zinc coatings, the latter were developed in comparable conditions to those used for the Zn–Co deposits (Table 2, Solution E). Figure 8 shows that SEM micrographs reveal the typical structure of zinc with the development of hexagonal platelets of different sizes. According to these micrographs, especially when compared to those of Zn–Co coatings (Figure 7), the Co effect on coating deposition is particularly notable, allowing the structure to be refined from a hexagonal to a nodular and thin morphology. In fact, the cobalt is nobler than the zinc. Thus, when the cobalt begins to deposit, it tends to bind to zinc-rich sites, increasing the number of nucleation sites and promoting grain refinement [27,28].

Figure 9 shows the XRD diagrams obtained during the pure zinc and Zn–5 wt% Co coatings' analysis. Concerning pure zinc films (Figure 9a), patterns corresponding to zinc phase are detected at $2\theta = 38°$, 39°, 42°, 55°, 70°, and 82°. By alloying zinc with cobalt (Figure 9b), it is obvious that the corresponding peaks of pure zinc have become wider, implying a decrease in particle size. Moreover, the intensity of the most prominent peak occurring at $2\theta = 42°$ decreased from about 2700 to 1900 with the crystallization of the monoclinic intermetallic phase γ_2 ($CoZn_{13}$) at $2\theta = 41°$. This interpretation demonstrates the deconvolution of two peaks between $2\theta = 41°$ and $2\theta = 42°$. The intermetallic phase was also detected at 78°. The peak indicating the presence of iron emanates from the steel substrate.

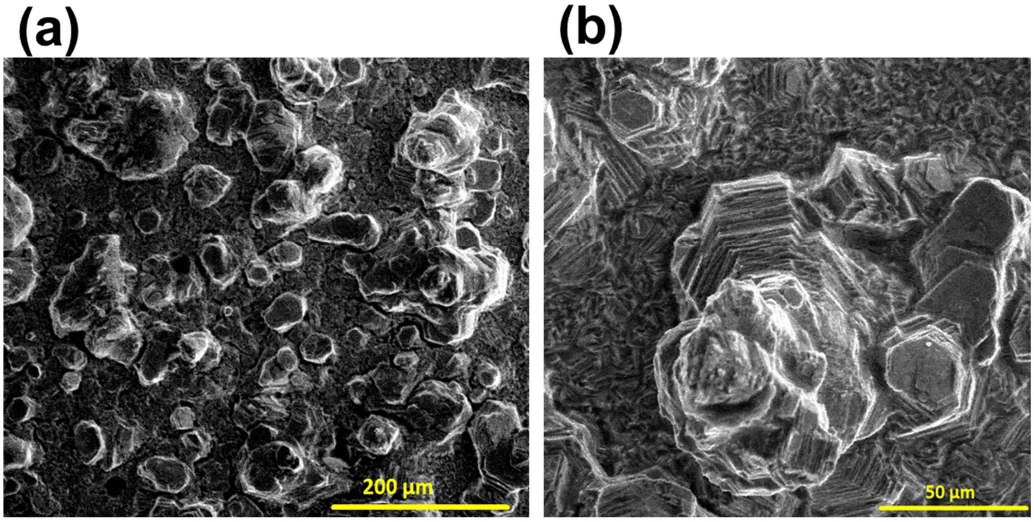

Figure 8. SEM micrographs of pure Zn at different magnifications; (**a**): 250× (**b**): 1000×.

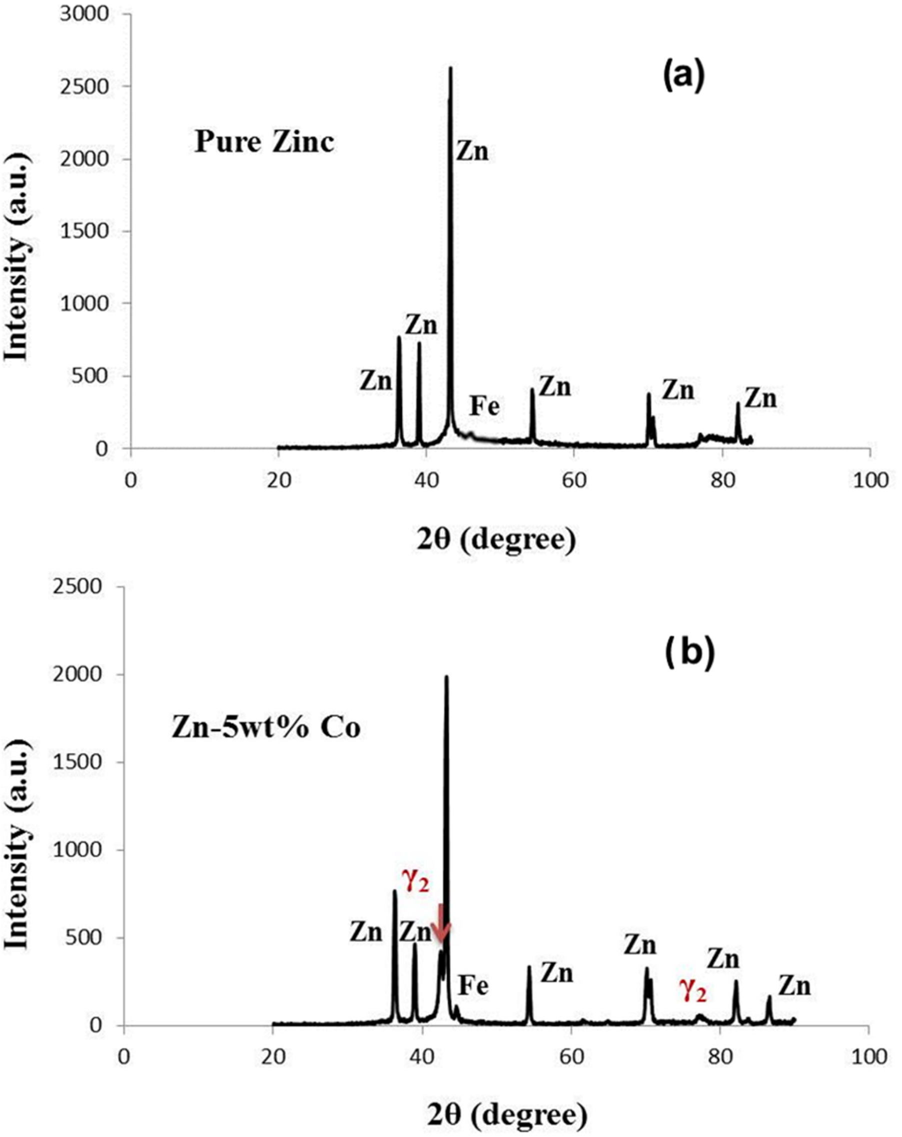

Figure 9. X-ray diffraction patterns of pure zinc coatings (**a**) and Zn–5 wt% Co coatings (**b**).

The obtained results reveal that Zn–Co alloy coatings are composed of pure zinc and a monoclinic intermetallic phase γ_2 ($CoZn_{13}$), which accords well with the Zn–Co phases' diagram [24]. In addition, the presence of monoclinic intermetallic phase γ_2 ($CoZn_{13}$) can be justified by the fact that alloy coatings include considerable content of cobalt (5 wt%) [29,30]. The average crystallite sizes of pure zinc and Zn–Co coatings calculated by the Debye–Scherrer equation were about 7 µm and 45 ± 5 nm, respectively.

Additionally, the volume fraction of zinc (V_Z) could be estimated using the following relation:

$$V_Z = \frac{I, A}{I, Aref}$$

where "I, A" is the height of the intense peak in the pure zinc sample and "I, Aref" is the height of the intense peak in the Zn–Co sample. So, the volume fraction was found to be in the order of 0.75 (75%).

Indeed, the integration of cobalt to zinc coatings allows for the transformation of the coatings structure from micrometric to nanometric scale despite the zinc's dominance over cobalt. The XRD analysis is in agreement with the previous SEM observations and cyclovoltametric study.

In the following section, pure zinc and Zn–5 wt% Co developed at 24 °C will be characterized by mechanical and tribological tests.

3.2. Mechanical and Tribological Characterization of Zinc and Zn–Co Coatings

3.2.1. Roughness and Microhardness

Table 3 shows the average values of Ra roughness and Hv microhardness for the various studied coatings, together with their standard deviations. Pure zinc layers appear to have the roughest surface (1.2 µm). However, Zn–Co coatings appear to have a smoother surface (0.5 µm). This result is in line with those obtained in previous SEM observations of different coatings' surface morphology.

Table 3. Roughness and microhardness values of pure zinc and Zn–Co coatings.

	Pure Zinc	Zn–Co Alloys
Roughness (µm)	1.2 ± 0.2	0.5 ± 0.1
Microhardness (Hv)	106.5 ± 7.0	123 ± 4.0

According to Table 3, microhardness results indicate that pure zinc coatings exhibit lower hardness (106.5 Hv), while Zn–Co layers demonstrate a significantly harder surface (123 Hv). Alloying zinc with cobalt enhanced the coatings' hardness, which can be attributed to cobalt's ability to refine the grain size. Hence, under the bath conditions used, the addition of cobalt to pure zinc led to a reduction in the grain size. The SEM images in Figures 7 and 8 show that the presence of cobalt, under appropriate conditions, results in a smoother, more homogeneous and finer morphology compared to pure zinc. According to Hall–Pecth's law, the reduction in grain size prevents the dislocation movement, thereby increasing microhardness [31].

3.2.2. Friction and Wear Properties

Table 4 exhibits the stabilized values of the friction coefficient and wear volume loss for pure zinc and Zn–Co coatings, along with their standard deviations. The results reveal that after 5000 sliding cycles, pure zinc coatings present the highest friction coefficient. The high value of friction coefficient (0.66) of pure zinc layers can be attributed to its large size structure, important roughness, and particularly its low hardness, which enhance surface interaction and, consequently, significantly increase the friction. However, alloying zinc with a nobler metal greatly improved the friction response of zinc coatings. Therefore, the friction coefficient decreased from 0.66 to 0.31 for the Zn–Co layers, owing to the smoother and least-rough surface of alloy coatings.

Table 4. Friction coefficient and wear volume loss values of pure Zn and Zn–Co coatings.

	Pure Zinc	Zn–Co Alloys
Friction Coefficient	0.66 ± 0.02	0.31 ± 0.02
Wear Volume Loss (mm^3)	1 ± 0.08	0.58 ± 0.30

Additionally, the calculated wear volume loss presented in Table 4 affirms that adding cobalt allows for the inhibition of wear mechanisms to develop, and therefore, decreases the wear volume loss substantially from 1 to 0.58 mm^3. The obtained finding may be associated with the coating's microhardness values as the Zn–Co coating's surfaces are harder than pure zinc layers. Indeed, alloying zinc with cobalt leads to the reinforcement of the coating's microhardness, and thus the enhancement of the wear resistance of zinc layers. Indeed, the Zn–Co coatings represent the best wear resistance thanks to them having the lowest friction coefficient and highest microhardness. This result aligns with "Archard's theory", which predicts that, under specific mechanisms, an increase in hardness leads to improved wear resistance [32].

According to the literature, depositing Zn–4 wt% Co coatings on mild steel using sodium as an additive and adjusting the pH up to 1.5 permitted the development of films with a nodular grain shape and few microcracks [25], with a microhardness measurement of about 105 Hv. Using the same electrolytic bath but with copper as a substrate yielded coatings with a microhardness of 85 Hv [24]. However, coatings developed under our specific conditions, despite having a similar cobalt content (5 wt%), exhibited improved properties. The morphology seemed to be typically nodular and finer, with a greater reduction in grain size and a non-cracked surface. In addition, the surface hardness was significantly enhanced, reaching approximately 123 Hv. This finding holds significant importance for various industries (automotive, railway, aerospace, etc.), where metal components are always exposed to corrosion and wear, especially when used in sliding contacts. To extend the service lifespan of these components, various coating materials and processes are used. Zinc demonstrates good wettability, which improves the interfacial bonding characteristics between the coating and the substrate [12]. Hence, the development of nanostructured Zn-based coatings by adding cobalt may enhance further the mechanical and tribological performances of those coatings.

As a perspective for future work, we aim to develop nanostructured Zn–Co alloy coatings with varied cobalt content (below and above 5 wt%) using the same methodology developed in this study. Microstructure analysis, micromechanical characterization, and tribological evaluations will be carried out to optimize the coating performance.

4. Conclusions

The morphological evolution, microstructure, micromechanical, and tribological properties of pure zinc and Zn–Co coatings electrodeposited on mild steel substrates, can be refined into the following essential points:

(1) At a room temperature of 17 °C, the addition of salt significantly improved cobalt electrocrystallization, resulting in nodular and uniform Zn–Co coatings.

(2) pH adjustment guaranteed the homogenization and refinement of Zn–Co layers with only 5 wt.% of cobalt content, on the one hand, and the reduction of only two crystallized phases, on the other.

(3) Using 24 °C as room temperature allowed us to deposit alloy coatings with a nodular and remarkably smoother structure, keeping the resulting nodular and smoother alloy coatings while maintaining the same cobalt content (5 wt.%) as at 17 °C.

(4) By adding cobalt, the morphology of pure zinc coatings changed from hexagonal platelets to a typical nodular structure, with the crystallization of monoclinic intermetallic phase γ_2 ($CoZn_{13}$) permitting the reduction in grain size from micrometre (7 μm) to nanometre scale (45 nm).

(5) Alloying zinc with cobalt markedly improved not only the surface quality in terms of roughness, but also the microhardness. This was done by developing alloy coatings which are harder than pure zinc layers.

(6) The upgrade of mechanical characteristics led to an improved of friction response and wear mechanism development by mitigating the friction coefficient and the wear volume loss of pure zinc coatings.

(7) Zn–5 wt% Co coatings presented the best micromechanical qualities and wear resistance, revealing a smooth and hard surface with a nodular nanocrystalline morphology.

Author Contributions: Methodology, F.N.; validation, M.K. and F.V.; resources, A.P. and C.C.; writing—original draft, F.N. and D.T.; writing—review and editing, M.K. and M.D.; supervision, A.P.; project administration, C.C.; funding acquisition, A.P. All authors have read and agreed to the published version of the manuscript.

Funding: This work was developed in the scope of the Project AM2R—Agenda Mobilizadora para a inovação empresarial do setor das Duas Rodas [C644866475-00000012—project n. 15], financed by PRR—Recovery and Resilience Plan under the Next Generation EU from the European Union, and has laboratory support from the projects UIDB/00481/2020 and UIDP/00481/2020-FCT-Fundação para a Ciência e a Tecnologia.

Data Availability Statement: Data is contained within the article.

Conflicts of Interest: Author C.C. was employed by the company Rodi Industries. The remaining authors declare that the research was conducted in the absence of any commercial or financial relationships that could be construed as a potential conflict of interest.

References

1. Boshkov, N. Influence of the alloying component on the protective ability of some zinc galvanic coatings. *Electrochim. Acta* **2005**, *51*, 7–84.
2. Karahan, I.H.; Guder, H.S. Electrodeposition and properties of Zn, Zn-Ni, Zn-Fe and Zn-Fe-Ni alloys from acidic chloride-sulphate electrolytes. *Trans. IMF* **2009**, *87*, 155–158.
3. Abou-Krisha, M.M.; Assaf, F.H.; Toghan, A.A. Electrodeposition of Zn–Ni alloys from sulfate bath. *J. Solid State Elelchtrochem.* **2007**, *11*, 244–252.
4. Nasri, F.; Zouari, M.; Kharrat, M.; Dammak, M.; Vacandio, F.; Eyraud, M. Structural, Micromechanical and Tribological Characterization of Zn–Ni Coatings: Effect of Sulfate Bath Composition. *Trans. Indian Inst. Met.* **2018**, *71*, 1827–1840.
5. Karahan, I.H.; Karabulut, O.; Alver, U. A study on electrodeposited Zn–Co alloys. *Phys. Scr.* **2009**, *79*, 055801.
6. Garcia, J.R.; do Lago, D.C.B.; de Senna, L.F. Electrodeposition of Cobalt Rich Zn-Co alloy Coatings from Citrate Bath. *Mater. Res.* **2014**, *17*, 947–957.
7. Lv, Y.; Cai, G.; Zhang, X.; Fu, S.; Zhang, E.; Yang, L.; Xiao, J.; Dong, Z. Microstructural characterization and in vitro biological performances of Ag, Zn co-incorporated TiO_2 coating. *Ceram. Int.* **2020**, *46*, 29160–29172.
8. Zhang, J.; Dai, J.-Q.; Zhang, G.-C.; Zhu, X.-J. Significantly improved ferroelectric properties of (Zn,Co) co-doped $BiFeO_3$ thin films prepared by sol-gel method. *Ceram. Int.* **2024**, *50*, 28449–28457.
9. Tahraoui, L. Effet de la Concentration de Cr sur l'électrodéposition d'un Dépôt Composite Zn-Co-Cr. Ph.D. Thesis, Université de Mohamed Khider Biskra, Biskra, Algeria, 2021.
10. Yavuz, A.; Yilmaz Erdogan, P.; Zengin, H.; Zengin, G. Electrodeposition and Characterisation of Zn-Co Alloys from Ionic Liquids on Copper. *J. Electron. Mater.* **2022**, *51*, 5253–5261.

11. Bhat, R.S.; Manjunatha, K.B.; Venkatakrishna, K.; Chitharanjan Hegde, A. Electrodeposition of Zn–Co Coating and its Electrochemical Performance. *Prot. Met. Phys. Chem. Surf.* **2022**, *58*, 99–108.
12. Sundaramali, G.; Aiyasamy, J.; Karthikeyan, S.; Kandavel, T.; Arulmurugan, B.; Rajkumar, S.; Sharma, S.; Li, C.; Dwivedi, S.; Kumar, A.; et al. Experimental investigations of electrodeposited Zn–Ni, Zn–Co, and Ni–Cr–Co–based novel coatings on AA7075 substrate to ameliorate the mechanical, abrasion, morphological, and corrosion properties for automotive applications. *Rev. Adv. Mater. Sci.* **2023**, *62*, 20220324.
13. Heydari Gharahcheshmeh, M.; Heydarzadeh Sohi, M. Study of the corrosion behavior of zinc and Zn-Co alloy electrodeposits obtained from alkaline bath using direct current. *Mater. Chem. Phys.* **2009**, *117*, 414–421.
14. Ortiz, Z.I.; Diaz-Arista, P.; Meas, Y.; Ortega-Borges, R.; Trejo, G. Characterization of the corrosion products of electrodeposited Zn; Zn-Co and Zn-Mn alloys coatings. *Corros. Sci.* **2009**, *51*, 2703–2715.
15. Bajat, J.B.; Stanković, S.; Jokić, B.M.; Stevanović, S.I. Corrosion stability of Zn–Co alloys deposited from baths with high and low Co content—The influence of deposition current density. *Surf. Coat. Technol.* **2010**, *204*, 2745–2753.
16. Lichušina, S.; Sudavičius, A.; Juškenas, R.; Bučinskiene, D.; Juzeliūnas, E. Deposition of cobalt rich Zn–Co alloy coatings of high corrosion resistance. *Trans. IMF* **2008**, *86*, 141–147.
17. Toghan, A.; Abou-krisha, M.M.; Assaf, F.H.; El-Sheref, F. Effect of Deposition Potential on the Mechanism and Corrosion Behavior of Zn-Fe-Co Thin Coatings Electrochemically Deposited on a Steel Substrate. *Int. J. Electrochem. Sci.* **2021**, *16*, 151044.
18. Garcia, J.R.; do Lago, D.C.B.; Cesar, D.V.; de Senna, L.F. Pulsed cobalt-rich Zn–Co alloy coatings produced from citrate baths. *Surf. Coat. Technol.* **2016**, *306*, 462–472.
19. Falcón, J.M.; Aoki, I.V. Electrodeposition of Zn-Co alloy coatings on carbon steel and their corrosion resistance. *Surf. Coat. Technol.* **2024**, *481*, 130603.
20. Lodhi, Z.F.; Tichelaar, F.D.; Kwakernaak, C.; Mol, J.M.C.; Terryn, H.; de Wit, J.H.W. A combined composition and morphology study of electrodeposited Zn–Co and Zn–Co–Fe alloy coatings. *Surf. Coat. Technol.* **2008**, *202*, 2755–2764.
21. Dikici, T.; Culha, O.; Toparli, M. Study of the mechanical and structural properties of Zn–Ni–Co ternary alloy electroplating. *J. Coat. Technol. Res.* **2010**, *7*, 787–792. [CrossRef]
22. Kahloul, A.; Azizi, F.; Bouaoud, M. Effect of citrate additive on the electrodeposition and corrosion behaviour of Zn–Co alloy. *Trans. IMF* **2017**, *95*, 106–113. [CrossRef]
23. Chu, Q.; Wang, W.; Liang, J.; Hao, J.; Zhen, Z. Electrodeposition of high Co content nanocrystalline Zn–Co alloys from a choline chloride-based ionic liquid. *Mater. Chem. Phys.* **2013**, *142*, 539–544.
24. Panagopoulos, C.N.; Georgarakis, K.G.; Petroutzakou, S. Sliding wear behaviour of zinc–cobalt alloy electrodeposits. *J. Mater. Process. Technol.* **2005**, *160*, 234–244. [CrossRef]
25. Panagopoulos, C.N.; Largis, D.A.; Vatista, P.C. Adhesion and corrosion behavior of Zn-Co electrodeposits on mild steel. *Mater. Chem. Phys.* **2011**, *126*, 398–403. [CrossRef]
26. Caprentier, L. Caractérisation Micromécanique de Matériaux Composites et Anisotropes par Indentation Instrumentée. Ph.D. Thesis, Ecole Centrale de Lyon, Lyon, France, 1994.
27. Heydari Gharahcheshmeh, M.; Heydarzadeh Sohi, M. Electrochemical studies of zinc–cobalt alloy coatings deposited from alkaline baths containing glycine as complexing agent. *J. Appl. Electrochem.* **2010**, *40*, 1563–1570. [CrossRef]
28. Yi, L.; Wang, S.; Wood, R.J.K. Controlled Compositions in Zn–Ni Coatings by Anode Material Selection for Replacing Cadmium. *Coatings* **2024**, *14*, 1119. [CrossRef]
29. Gómez, E.; Alcobe, X.; Vallés, E. Characterisation of zinc + cobalt alloy phases obtained by electrodeposition. *J. Electroanal. Chem.* **2001**, *505*, 54–61.
30. Rashwan, S.M.; Mohamed, A.E.; Abdel-Wahaab, S.M.; Kamel, M.M. Electrodeposition and characterization of thin layers of Zn–Co alloys obtained from glycinate baths. *J. Appl. Electrochem.* **2003**, *33*, 1035–1042. [CrossRef]
31. Brooks, I.; Erb, U. Hardness of electrodeposited microcrystalline and nanocrystalline gamma-phase Zn-Ni alloys. *Scr. Mater.* **2001**, *44*, 853–858. [CrossRef]
32. Hutchings, I.M. *Tribology: Friction and Wear of Engineering Materials*; CRC Press: London, UK, 1992.